bioRxiv preprint doi: https://doi.org/10.1101/2022.07.27.500934; this version posted October 19, 2022. The copyright holder for this preprint (which was not certified by peer review) is the author/funder, who has granted bioRxiv a license to display the preprint in perpetuity. It is made available under aCC-BY 4.0 International license.

The anatomy of transcriptionally active chromatin loops in *Drosophila* primary spermatocytes using super-resolution microscopy

Madeleine L. Ball[1†], Stefan A. Koestler[1†], Leila Muresan[2], Sohaib Abdul Rehman[2,3], Kevin O'Holleran[2] and Robert White[1*]

[1]Department of Physiology, Development and Neuroscience, University of Cambridge, Downing Site, Cambridge, CB2 3DY, UK.
[2]Cambridge Advanced Imaging Centre, University of Cambridge, Downing Site, Cambridge, CB2 3DY, UK
[3]Current address: Department of Molecular and Cellular Biology, Harvard University, Cambridge, MA 02138, USA
[†] These authors contributed equally
[*] Corresponding author (rw108@cam.ac.uk)

Abstract

While the biochemistry of gene transcription has been well studied, our understanding of how this process is organised in 3D within the intact nucleus is less well understood. Here we investigate the structure of actively transcribed chromatin and the architecture of its interaction with active RNA polymerase.

For this analysis, we have used super-resolution microscopy to image the *Drosophila melanogaster* Y loops which represent huge, several megabases long, single transcription units. The Y loops provide a particularly amenable model system for transcriptionally active chromatin. We find that, although these transcribed loops are decondensed they are not organised as extended 10nm fibres, but rather they largely consist of chains of nucleosome clusters. The average width of each cluster is around 50nm. We find that foci of active RNA polymerase are generally located off the main fibre axis on the periphery of the nucleosome clusters. Foci of RNA polymerase and nascent transcripts are distributed around the Y loops rather than being clustered in individual transcription factories. However, as the RNA polymerase foci are considerably less prevalent than the nucleosome clusters, the organisation of this active chromatin into chains of nucleosome clusters is unlikely to be determined by the activity of the polymerases transcribing the Y loops.

These results provide a foundation for understanding the topological relationship between chromatin and the process of gene transcription.

Keywords: Nuclear organisation, Chromatin, Transcription, Super-resolution microscopy, RNA polymerase II, Nucleosome

Introduction

Considerable advances have been made recently in understanding the organisation of chromatin in the nucleus and its relevance for the function and regulation of the genome (for a recent review see (1)). Genomic studies have provided insights into the variety of levels of organisation ranging from chromatin loops (2,3) and topologically associated domains (4,5), to spatially segregated compartments of condensed repressed chromatin and decondensed active chromatin (6) and chromosome territories (7). Imaging approaches have provided a complementary view, revealing a dynamic landscape of chromatin structures associated with transcription and replication (8,9). A fundamental insight emerged from EM studies indicating that chromatin forms a disordered chain within the interphase nucleus with a variety of local structural motifs based on configurations of the 10nm nucleosomal fibre (10). Other studies have revealed that chromatin is locally organised into small nucleosomal clusters of various sizes (variously termed clutches or domains (11,12)) and super-resolution microscopy has begun to define the structural characteristics of different chromatin states (13,14). However, linking specific chromatin configurations to the different activities carried out by chromatin remains an important objective if we are to understand how the structure of chromatin facilitates and regulates its many functions. For example, transcriptional activation has long been associated with chromatin decondensation (15–19) but we know little of the detailed chromatin environment encountered by an elongating polymerase.

Imaging chromatin structure within the nucleus is, however, challenging as in most nuclei chromatin is densely packed. Here we take advantage of the exceptionally large nuclei of *Drosophila* primary spermatocytes which show an ordered arrangement of separate chromosomes and a large nucleoplasmic space (20,21). Much of the nucleoplasm is engaged in the transcription of just a few genes on the Y-chromosome, the enormous genes of the Y loops. These genes, which are specifically activated in the primary spermatocytes, provide an attractive model for the study of transcriptionally active chromatin. The three genes, *kl-5*, *kl-3* and *ks-1*, decondense upon activation and extend as Y loops in the nucleoplasm (20–22). These Y loop genes are transcribed as single transcription units, several megabases in length (23,24). For example, one of these Y loop genes, *kl-3*

bioRxiv preprint doi: https://doi.org/10.1101/2022.07.27.500934; this version posted October 19, 2022. The copyright holder for this preprint (which was not certified by peer review) is the author/funder, who has granted bioRxiv a license to display the preprint in perpetuity. It is made available under aCC-BY 4.0 International license.

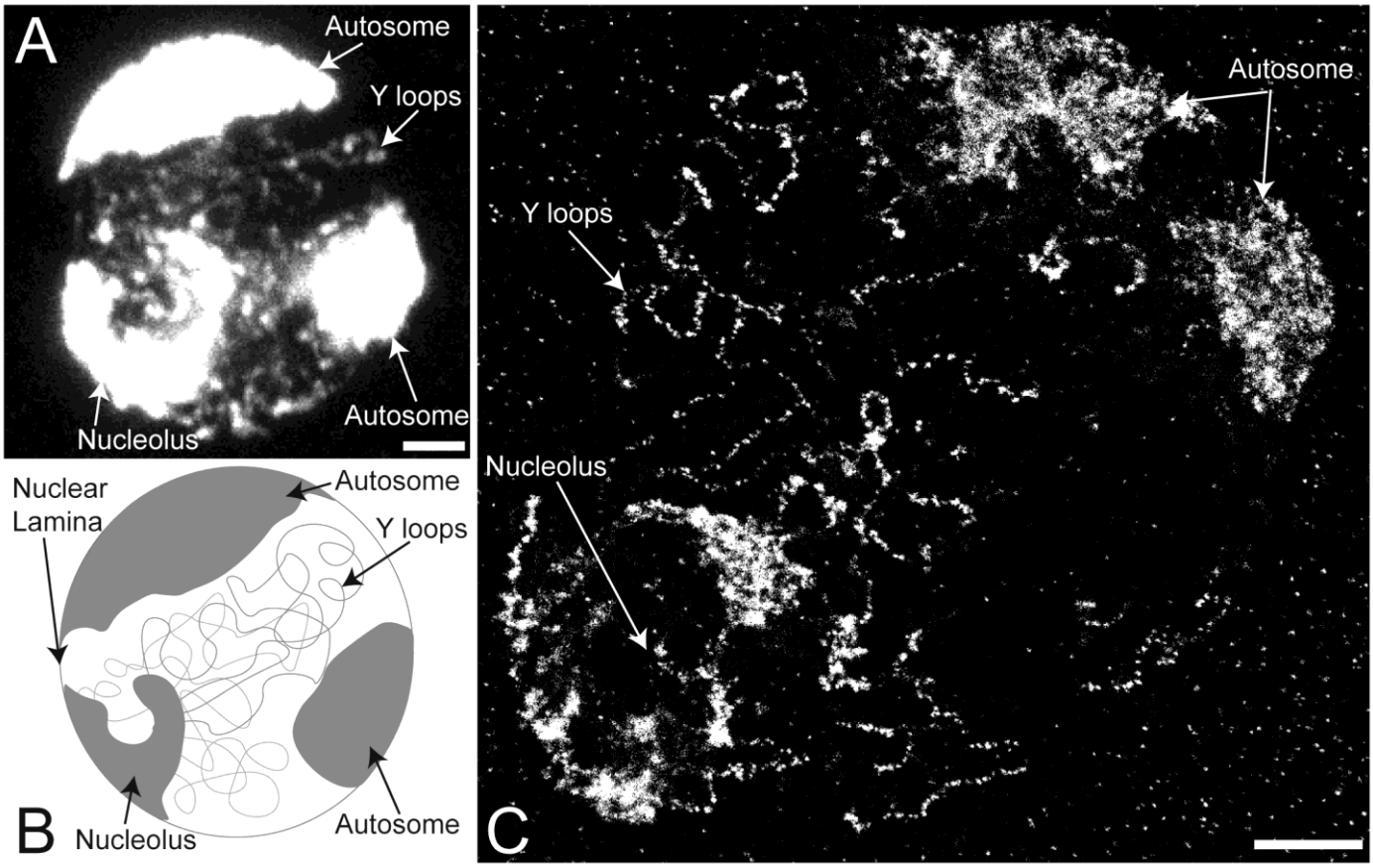

Figure 1. Overview of the *Drosophila* primary spermatocyte nucleus. (A) Confocal image of *Drosophila* primary spermatocyte nucleus immunolabelled with pan-histone antibody labelling core histones plus H1. **(B)** Schematic showing the characteristic features of the *Drosophila* primary spermatocyte nuclei. **(C)** STORM super-resolution image of *Drosophila* primary spermatocyte nucleus, immunolabelled with pan-histone antibody. The Y loops, nucleolus, and two lobes of the same autosome are indicated with arrows. Scale bars are 2 µm.

which encodes an axonemal dynein heavy chain spans at least 4.3Mb, although most of this sequence is intronic and its coding sequence is only ~14kb (20,22–24). These Y loops, easily visible in phase-contrast light microscopy, have long been recognised as models for the organisation of transcriptionally active chromatin providing a paradigm for gene activation, chromatin decondensation, loop formation and the topology of RNA polymerase progression (15).

In this study, we have focused on the use of super-resolution microscopy to investigate the chromatin structure of Y loops and its relationship to transcription. We find that the chromatin fibre in these transcriptionally active loops is not simply extended as a 10nm fibre but rather is largely organised as a chain of nucleosomal clusters. RNA polymerase is associated with the periphery of these clusters. Comparison of the nucleosome cluster versus RNA polymerase prevalence suggests that the chromatin clustering is not generated by RNA polymerase activity between the clusters. It appears that the chain of nucleosomal clusters forms the basic structure of decondensed chromatin upon which RNA polymerase acts.

Results

The fine structure of Y loop chromatin

In *Drosophila* spermatogenesis, after the last spermatogonial mitosis, the primary spermatocytes enter a G2 phase that lasts for several days. In this period they expand over 20-fold in volume and activate the spermatogenesis transcription program. As part of this program, three individual Y chromosome genes decondense from the Y chromosome mass, which is located close to the nucleolus, and spill out into the nucleoplasm forming the Y loops. These actively transcribed loops can be easily visualised by DNA labelling or anti-histone immunolabelling and in confocal microscopy, the loops appear as chromatin ribbons that follow convoluted paths within the nucleus (Fig 1A,B). Close examination indicates that these ribbons may not have a uniform structure and often they exhibit a “chain of blobs” appearance. To investigate the structure of this transcriptionally active chromatin in more detail we have examined the loops in super-resolution using Stochastic Optical Reconstruction Microscopy (STORM) (25).

STORM imaging of Y loop chromatin labelled with anti-histone antibody reveals the fine structure of the Y loops predominantly as chains of small chromatin clusters (Fig 1C). At higher magnification (Fig 2) sparse localisations can be seen in the “links” between the clusters indicating that the linking chromatin is also nucleosomal. Using a series of z-slices to sample a z-depth of over 1.5µm demonstrates that the clustered appearance of the Y loop chromatin represents genuine 3D clusters and is not due to optical sectioning of a restricted focal depth (Fig 2).

To model the spatial aggregation of antibody labelled nucleosomes within the Y loop clusters, several clustering methods were considered to identify and describe the variability in cluster sizes; including DBSCAN (26), a Bayesian approach (27) and the mode-finding clustering algorithm MeanShift (28–30). We found MeanShift to be more robust than the alternatives (26,27,31) with respect to identifying clusters closely positioned along a fibre. The crucial input parameter of MeanShift

bioRxiv preprint doi: https://doi.org/10.1101/2022.07.27.500934; this version posted October 19, 2022. The copyright holder for this preprint (which was not certified by peer review) is the author/funder, who has granted bioRxiv a license to display the preprint in perpetuity. It is made available under aCC-BY 4.0 International license.

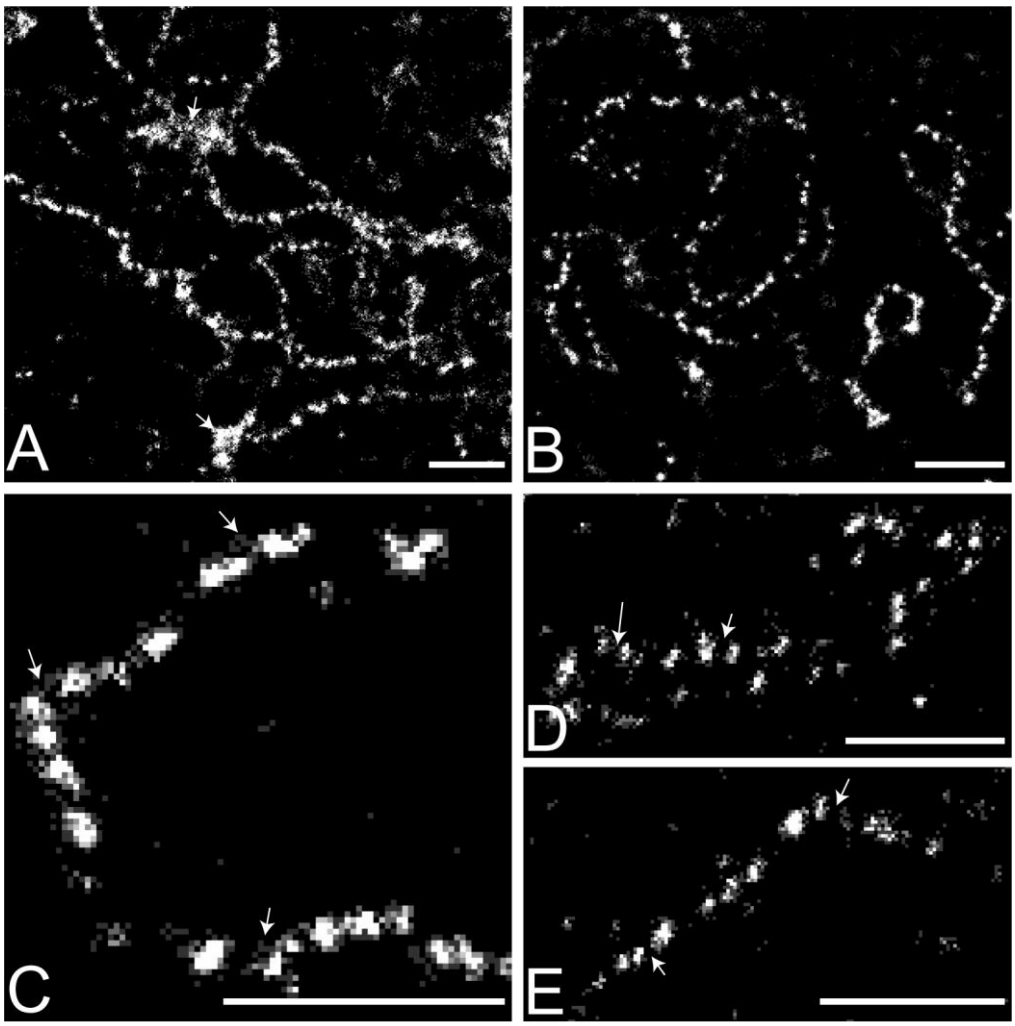

Figure 2. STORM super-resolution images of the Y loops.
Histones are immunolabelled with pan-histone antibody, showing the clusters of nucleosomes. **(A-C)** Three representative examples of single slice images from different cells are shown increasing in magnification from A to C. The Y loops are largely made up of semi-regular clusters of nucleosomes. In A there are also some larger aggregates visible, indicated with arrows. In C the arrows indicate evidence of smaller looping regions of chromatin fibres between and extending from the nucleosome clusters. **(D and E)** Maximum projection images over 1.5 µm of Y loop fibres showing that the clusters are genuine 3D objects as the regions in between clusters of nucleosomes do not fill in and form a complete contiguous fibre; examples indicated with arrows. Scale bars are 1 µm.

is the search radius. In order to estimate the search radius an average cluster model was identified from the data based on spatial statistics modelling (see Materials and Methods for details), similar to approaches used previously (31–33). Using this spatial statistics and MeanShift approach to estimate cluster size, the median cluster width (Full Width Half Maximum, FWHM) is 52nm, with an interquartile range from 44nm to 61nm (Fig 3). The median distance between cluster centres is 107nm (Fig 4). On a simple volume calculation, a sphere of diameter 52nm could accommodate a maximum of 158 nucleosomes, however the density of nucleosomes in the clusters is likely to be much less than this. From EM studies, the chromatin volume concentration (CVC) ranges from 12 to 52% in interphase chromatin, with a mean of 30%, and in heterochromatin the range is 37 to 52% (10). It is not clear what CVC is appropriate for the Y loop clusters but, to provide an estimate of nucleosome number, taking a CVC value of 35% (above the mean but below the value for heterochromatin) would give a median of 54 nucleosomes per cluster (see Materials and Methods for details). The overall suggested structure is schematically diagrammed in Fig 4.

We note that although much of the Y loop chromatin adopts this "chain of clusters" structure, the Y loops do not simply have a uniform structure and, in addition to the individual elongated "chain of clusters" fibres, we also find regions of more aggregated chromatin (Figs 1 and 2).

Topology of active transcription

The observation that actively transcribed chromatin adopts a cluster chain organisation raises the question of the relationship of the clusters to active RNA polymerase. To examine this we used two-colour STORM microscopy with immunolabelling for RNA polymerase II with the phospho-Ser2 modification on the C-terminal domain repeats (RPol-PSer2) representing actively elongating RNA polymerase, together with anti-histone labelling for chromatin. We anticipated that elongating RNA polymerase might occupy the linking regions between the Y loop chromatin clusters however the labelling was surprising in two ways; first, the RPol-PSer2 labelling was sparse relative to the occurrence of cluster linking regions and second, the RPol-PSer2 labelling was not on the main chromatin fibre axis, rather the RPol-PSer2 localisation was peripherally associated with chromatin clusters (Fig 5). The first observation suggests that the cluster chain organisation is not dictated by the distribution of active polymerase and the second indicates a specific novel topological relationship between the cluster chain and the organisation of foci of active transcription. We confirmed that the observed displacement of the RPol-PSer2 localisations from the fibre axis was not due to camera misalignment (Suppl Fig 1). The distance of RPol-PSer2 from the main fibre axis shows quite a broad distribution with an average value of 100nm and the individual RPol-PSer2 foci have a median width of 48nm (Fig 6). The chromatin clusters are often associated with sparse anti-histone localisations surrounding the dense cluster core; these may represent decondensed loops emanating from the clusters and active polymerase complexes associated with the periphery of clusters may be engaged with these loop regions (Fig 5). We note that RPol-PSer2 is not only associated with the extended cluster chain regions of the Y loops but is also found on the surface of larger chromatin aggregates.

bioRxiv preprint doi: https://doi.org/10.1101/2022.07.27.500934; this version posted October 19, 2022. The copyright holder for this preprint (which was not certified by peer review) is the author/funder, who has granted bioRxiv a license to display the preprint in perpetuity. It is made available under aCC-BY 4.0 International license.

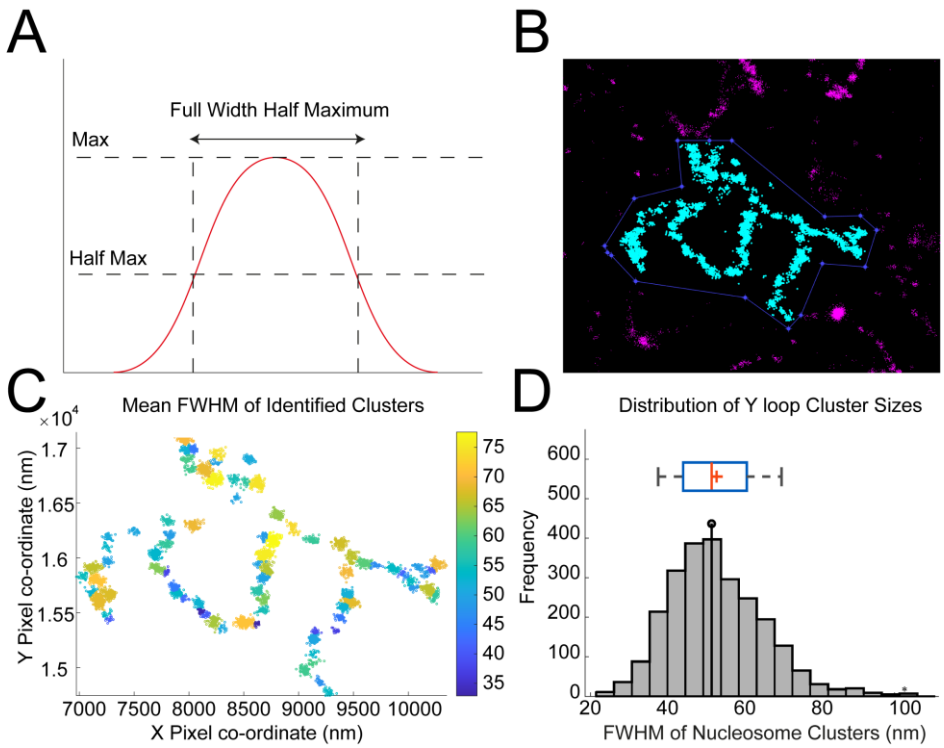

Figure 3. Quantification of chromatin clusters of the Y loops.
(A) A graphical representation of a theoretical Full Width Half Maximum (FWHM). The width of the distribution is taken at point of half the maximum signal. This is a measure of diameter that can exclude less confident edge points. **(B)** To quantify the sizes of the clusters along the Y loops, 32 regions of interest (ROI) were selected from 12 cells with the highest resolution, and with many Y loops visible, resulting in a total of 2473 clusters for analysis. **(C)** Pair Correlation Function (PCF) fitting was used to estimate the optimal search radius input, then the data were processed through the MeanShift algorithm to identify clusters. The heatmap scale is in nm. **(D)** The total distribution of FWHMs of the nucleosome clusters along the Y loops displayed with a histogram, and box and whiskers plot (the box indicates the inter-quartile range and the whiskers show the 9% and 91% bounds). The median FWHM was 52 nm, indicated with a lollipop on the histogram, and a line on the box and whiskers plot. The mean was 53 nm, indicated by a '+' on the box and whiskers plot.

As the RPol-PSer2 phosphorylated form of RNA polymerase may not represent all polymerase engaged on the Y loop chromatin, we also investigated the localisation of RNA polymerase II with the phospho-Ser5 modification on the C-terminal domain repeats (RPol-PSer5). The RPol-PSer5 phosphorylated form is associated with the initiation complex, paused polymerase and polymerase interacting with splicing complexes (34,35). As shown in Fig 7, RPol-PSer5 has a different distribution than RPol-PSer2 and much of the labelling in the nucleoplasm is dispersed and not clearly associated with chromatin fibres. Some labelling is associated with the Y loops but, as with RPol-PSer2, this is sparse relative to the clusters. We then investigated the combined occurrence of RPol-PSer2 and RPol-PSer5 using an antibody that labels both modified polymerase forms. The distribution of RPol-PSer2/PSer5 supports the above results (Fig 8), confirming that engaged RNA polymerase does not routinely occur in the cluster linking regions and also that the RNA polymerase localisations are on the periphery of the chromatin clusters and displaced from the main axis of the Y loop chromatin fibres.

Linking RNA polymerase distribution and Y loop transcription

The Y loops represent single transcription units whose large size provides an opportunity to investigate the organisation of nascent transcription in an active transcription loop. We have used the EU-Click-iT assay to image, by laser scanning confocal microscopy (LSCM), the nascent transcription occurring during a short time window (20min) of exposure of the testes to the EU nucleotide. We observe nascent transcription from Y loops as a series of blobs of EU incorporation distributed along extended lengths of the Y loop fibres (Fig 9). This distribution of nascent transcript along the Y loops fits with the distribution of RPol-PSer2, supporting the idea that the RPol-PSer2 localisations observed in the super-resolution images represent actively transcribing polymerase (Fig 5).

To further investigate the relationship between nascent transcription and the different modifications on the C-terminal domain of RNA polymerase II we have imaged RPol-PSer2 and RPol-PSer5 in association with EU Click-iT (Figs 9 and 10). The confocal images of RPol-PSer2 and RPol-PSer5 (Fig 9) provide an overview of the nuclear distribution of the two different modified polymerase forms. RPol-PSer2 is present in puncta on the autosome chromosome masses, on the sex chromosomes (X and Y) associated with the nucleolus and in trails of puncta associated with Y loops in the nucleoplasm. RPol-PSer5 has a similar distribution in puncta on the chromosome masses but has a distinct arrangement as a ring around the nucleolus and more puncta widely dispersed in the nucleoplasm. Imaging RPol-PSer2 together with nascent transcription confirms that RPol-PSer2 is associated with active elongation on the Y loops; as shown in the z-stack in Fig 10A the area of puncta of Y loop nascent transcription is closely associated with strong RPol-PSer2 labelling. In contrast, the Y loop nascent transcription is generally not associated with strong RPol-PSer5 signals and the weak dispersed puncta of RPol-PSer5 labelling in the nucleoplasm do not coincide with active nascent RNA production (Fig 10B). However, close to the nucleolus presumably at the start of a Y loop, a few strong puncta of RPol-PSer5 can be seen extending out from the nucleolus consistent with RPol-PSer5 association with the initiation of transcription. The Y loops thus enable us to visualise the distribution of the modified polymerase forms RPol-PSer2 and RPol-PSer5 along transcription units *in vivo* within intact nuclei.

Discussion

We have exploited the large size of the primary spermatocyte nuclei in *Drosophila* as a tractable model system for the super-resolution imaging of chromatin in intact nuclei. We have focussed on the organisation of transcriptionally active chromatin using the Y loop genes which are activated in spermatocytes and extend out from the Y chromosome into the nucleoplasm as

bioRxiv preprint doi: https://doi.org/10.1101/2022.07.27.500934; this version posted October 19, 2022. The copyright holder for this preprint (which was not certified by peer review) is the author/funder, who has granted bioRxiv a license to display the preprint in perpetuity. It is made available under aCC-BY 4.0 International license.

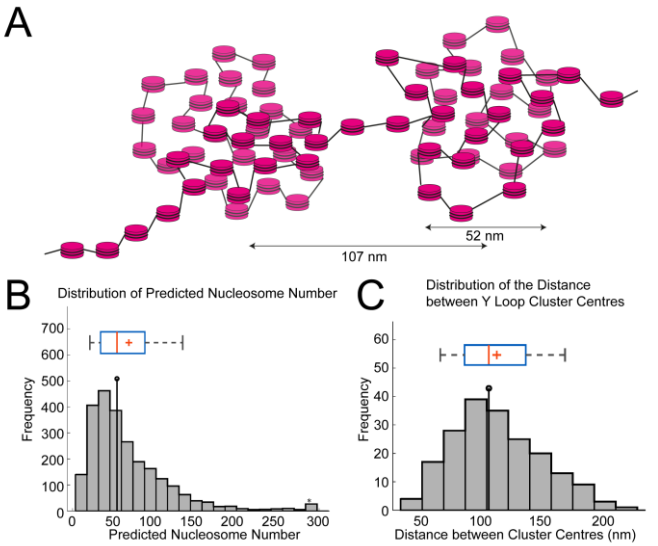

Figure 4. Estimating the number of nucleosomes in the Y loop clusters.
(A) Schematic of nucleosome clusters along the Y loops with nucleosomes depicted as magenta discs. The median FWHM of the clusters measured was 52 nm, shown here against a cluster as an example, as well as the median distance between cluster centres (107 nm). **(B)** Histogram showing the number of predicted nucleosomes within the measured clusters along the Y loops. The FWHM was used to estimate the maximum volume of the clusters and find the theoretical maximum of nucleosomes that would fit within that volume. 35% of this maximum was used as an estimate of nucleosome number based on how condensed the nucleosomes might be within these clusters. The median is 54. **(C)** Histogram of inter-cluster distance, the median is 107 nm. The box and whisker plots are as in Fig 3.

huge loops. We find that these active chromatin loops do not simply extend as 10nm "beads-on-a string" nucleosomal fibres but instead have a more complex structure and generally adopt an organisation as chains of nucleosome clusters. We have examined the relationship between this structure and the arrangement of RNA polymerase transcribing the loops and the organisation of nascent transcription.

The chromatin clusters have a relatively tight size distribution with a median width of 52nm and an interquartile range from 44-61nm. To estimate the width we have used the FWHM which provides a robust estimate of width, however it is an underestimate of the full width as the clusters do not have sharp perimeters. The lack of sharpness of the outer edge of clusters may be due to loosening of the compaction at the periphery or the formation of small loops of 10nm fibre extending from the compact clusters. In addition some of the uncertainty of the edge of the clusters will be due to the localisation precision of the STORM and also the labelling method, as the positions of the histones are visualised with an anti-histone primary antibody and a fluorophore-conjugated secondary antibody. Although this estimate is not a direct measurement, it provides a starting point for interpretation of the observed labelling in terms of underlying chromatin structure. As presented above in the Results, a chromatin cluster with a width of 52nm could accommodate 54 nucleosomes using a packing density (CVC of 35%) derived from EM analysis of nucleosome density in intact nuclei. In addition to the clusters, in the STORM images we also see sparse labelling between clusters indicating that the clusters are linked by nucleosomal chromatin and we also see localisations extending from the clusters supporting the occurrence of small chromatin loops emanating from the compact

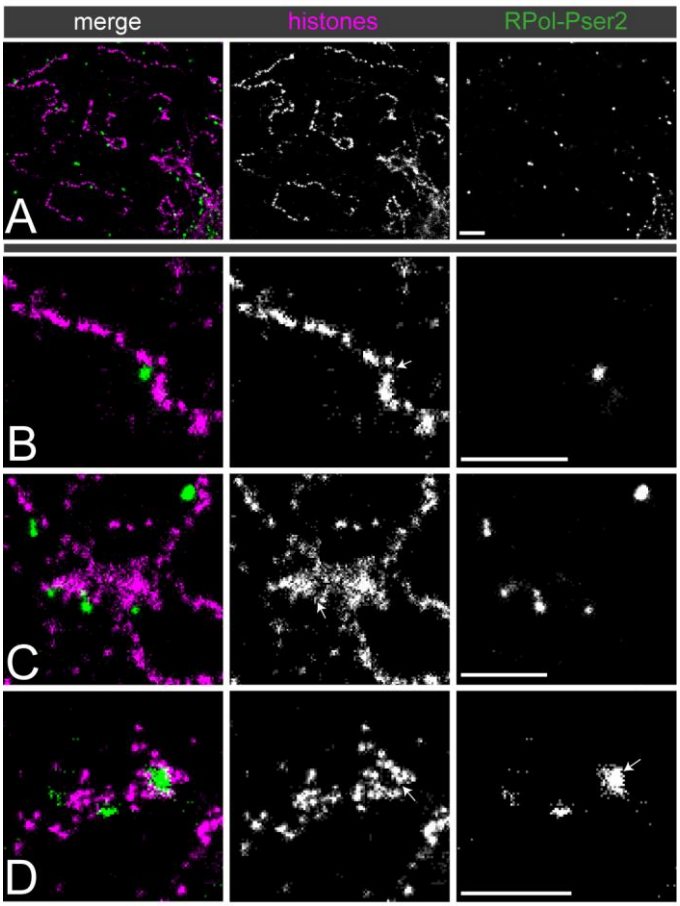

Figure 5. The association between Y loop chromatin clusters and active polymerase (RPol-PSer2).
Dual-colour STORM images of immunolabelled histones (magenta) and RPol-Pser2 (green). **(A)** gives an overview showing that polymerase foci are less prevalent than nucleosome clusters. (B to D) show selected examples at higher power. **(B)** An example of an individual Y loop fibre associated with one isolated focus of RPol-Pser2. RPol II appears to be associated with a looping region inbetween two nucleosome clusters, indicated with an arrow. **(C)** An example of larger aggregates of chromatin along the Y loops associated with RPol II. The foci of polymerase appear to be associated on the periphery of the aggregates, with some evidence of looping regions, indicated with an arrow. **(D)** An example of a larger focus of RPol II associated with Y loops. This larger focus could indicate a cluster of polymerase complexes co-transcribing as a "factory". These are rare to see, and do not seem to represent a universal organisation of transcription along the Y loops. Scale bars are 1µm.

clusters. Our interpretation of the overall structure is illustrated in the schematic in Fig 4.

To investigate the mechanism of cluster formation we asked whether the cluster linking regions might be sites of elongating polymerase as we considered that chromatin disruption or polymerase-dependent supercoiling might underpin the chromatin cluster chain organisation. However, elongating polymerase recognised by phosphorylation on Ser2 in the CTD repeats was too sparsely distributed on the loops to account for the chromatin cluster organisation. Even though the modified polymerase form associated with paused polymerase (RPol-PSer5) was more abundant than RPol-PSer2, neither its distribution nor the combined distributions of RPol-PSer2 and RPol-PSer2 indicated a fixed relationship between active polymerase and chromatin cluster formation. Thus our evidence does not support the idea that the cluster chain organisation is generated by transcription in the intervening regions. A similar conclusion was

bioRxiv preprint doi: https://doi.org/10.1101/2022.07.27.500934; this version posted October 19, 2022. The copyright holder for this preprint (which was not certified by peer review) is the author/funder, who has granted bioRxiv a license to display the preprint in perpetuity. It is made available under aCC-BY 4.0 International license.

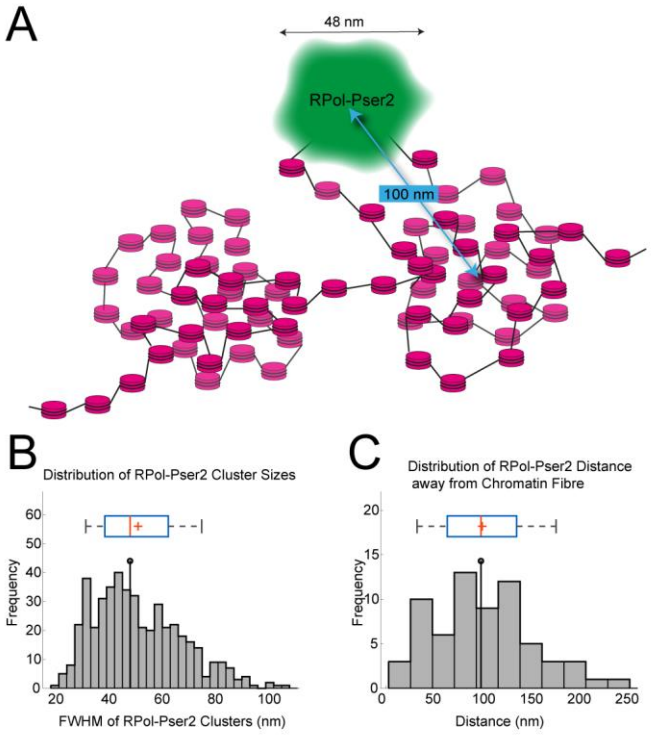

Figure 6. Quantification of association of Y loops to active transcription.
(A) Schematic showing interpretation of an individual polymerase focus (green) on the periphery of a nucleosome cluster, on a decondensed small loop extending from nucleosome cluster. Arrows indicate average width of polymerase foci and distance from focus centre to centre of nucleosome cluster. **(B)** Histogram of FWHM of polymerase foci. The median width is 48 nm. We note that the distribution appears biphasic or multiphasic suggesting the presence of multiple polymerases in each focus. **(C)** Histogram of distances between polymerase focus centre to centre of nucleosome cluster, mean is 100 nm. The box and whisker plots are as in Fig 3.

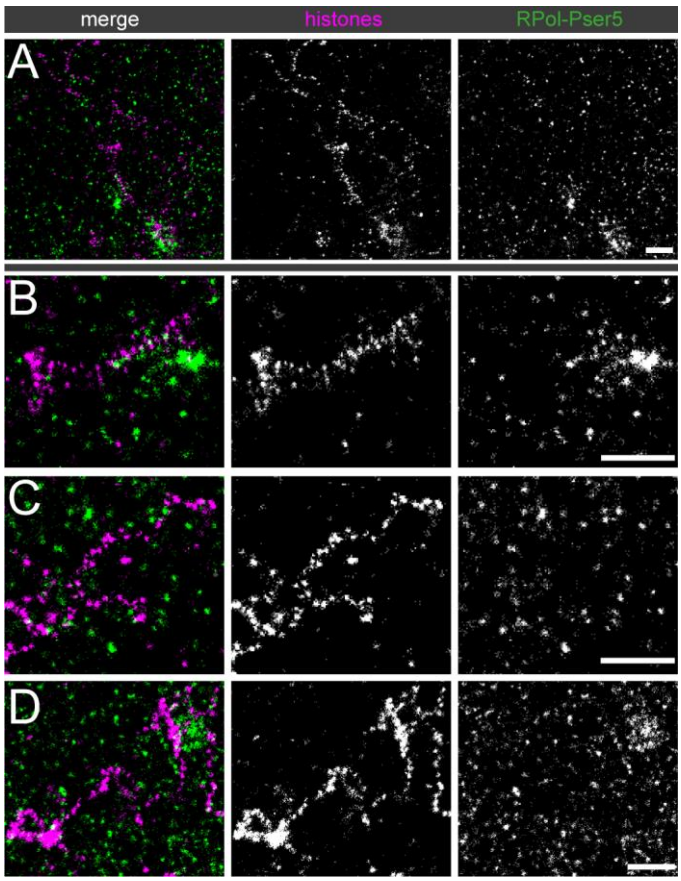

Figure 7. Association of Y loops to RPol-PSer5.
Dual-colour STORM images of immunolabelled histones (magenta) and RPol-Pser5 (green). **(A)** gives an overview and **(B to D)** show selected examples at higher power. Although RPol-PSer5 foci appear to be more prevalent than RPol-PSer2 foci, they are generally not present between the nucleosome clusters. In addition many RPol-PSer5 foci appear distant from chromatin fibres. Scale bars are 1µm.

reached by Castells-Garcia et al. (36) who suggested the independence of chromatin clutch formation and transcription. The cluster formation may represent an inherent self-aggregating property of chromatin as seen *in vitro* (37).

Examination of elongating polymerase (RPol-PSer2) in association with the chromatin fibre of the Y loops revealed an interesting topological relationship. The RPol-PSer2 is not simply associated with the central axis of the chromatin fibre but often is located off the fibre axis, on the periphery of a chromatin cluster (Fig 5 and schematic in Fig 6). In some cases the RPol-PSer2 is associated with sparse histone localisations extending from the chromatin clusters suggesting that the elongating polymerase is on a small chromatin loop. This arrangement of the elongating polymerase on the periphery of chromatin clusters fits with observations on mammalian cells (36), and may be relevant for the long-standing conundrum of how the polymerase transcribes double helical DNA without the transcript becoming entangled in the DNA. An attractive solution to this problem is that the polymerase is restrained from rotation, allowing the DNA to be reeled through the polymerase and so the transcript produced by this stable polymerase is not wound round the DNA (38,39). This then poses the question of how the polymerase might be stabilised. One potential solution is that the polymerases are aggregated into large transcription factories that provide the necessary structural restraint (40). Although we see occasional polymerase aggregates on the Y loops, in general the polymerase localisations are distributed along the loops and are not aggregated into large factories and this fits with the observation of nascent transcripts distributed in a series of blobs along the length of the Y loops (Fig 9). A similar distribution of nascent transcripts along chromatin loops is seen in long mammalian genes (41). The localisation of the elongating polymerase in a complex on the periphery of chromatin clusters could potentially provide stability and this, together with the association of a large mass of transcript RNP from these huge transcription units (42) may provide sufficient restraint from rotation.

The spermatocyte Y loop system also enabled us to examine the progression of the two phosphorylated forms of RNA polymerase (RPol-PSer2 and RPol-PSer5) on transcription units in intact nuclei. RPol-PSer2 is distributed over the Y loops and is associated with nascent transcript as expected for active elongating polymerase. RPol-PSer5 on the other hand is concentrated on the periphery of the nucleolus presumably where Y loop transcription is initiated, however it is also seen extending a short way out from the nucleolus (Fig 10) in a position consistent with association with the beginning of Y loop transcription. This suggests that the PSer5 modification is transiently retained on the elongating polymerase as it moves away from the site of initiation. We also find weak RPol-PSer5 signal widely dispersed in the nucleoplasm and in general this is not associated with active transcription; i.e. it is not associated with significant EU-Click-iT labelling in a 20min time window. Some

bioRxiv preprint doi: https://doi.org/10.1101/2022.07.27.500934; this version posted October 19, 2022. The copyright holder for this preprint (which was not certified by peer review) is the author/funder, who has granted bioRxiv a license to display the preprint in perpetuity. It is made available under aCC-BY 4.0 International license.

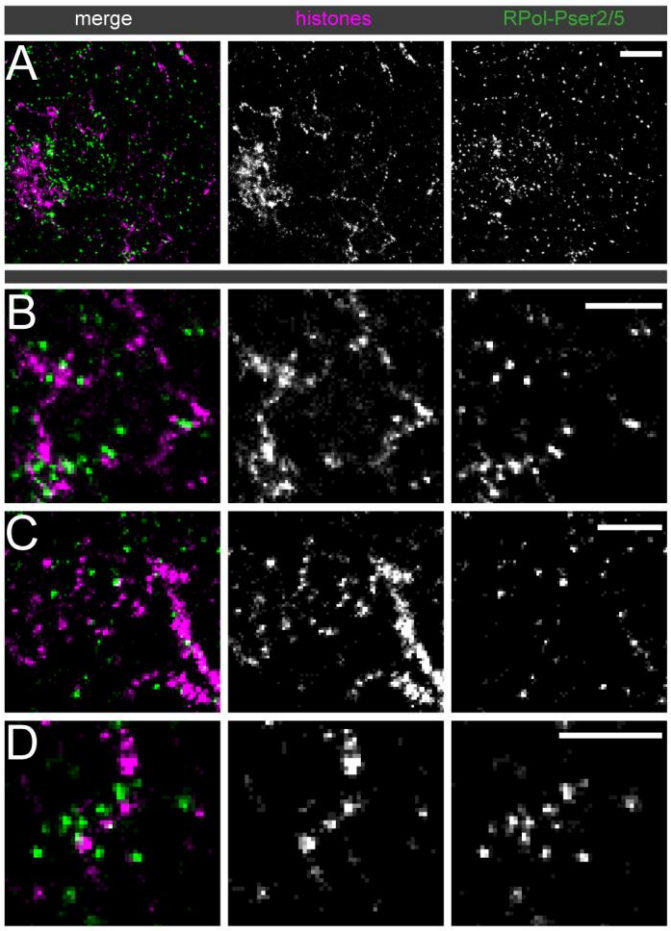

Figure 8. Association of Y loops to RPol-PSer2/PSer5.
Dual-colour STORM images of immunolabelled histones (magenta) and polymerase foci (green) using an antibody recognizing both RPol-Pser2 and RPol-PSer5. **(A)** gives an overview, scale bar is 1 µm and **(B to D)** show selected examples at higher power, scale bars are 500 nm. The polymerase foci are generally not present between the nucleosome clusters.

of this nucleoplasmic RPol-PSer5 is associated with Y loop chromatin fibres where it may indicate paused, stalled or slowed polymerase but much is also apparently distant from chromatin and the relevance of this non-chromatin-associated RPol-PSer5 is unclear. The strong RPol-PSer5 that extends a short way out from the nucleolus has the further implication that the site of initiation is positioned close to one end of the loop emerging from the Y chromosome located close to the nucleolus. The loops may thus be co-extensive with the transcription units which would be consistent with a role for transcription in the process of loop extension.

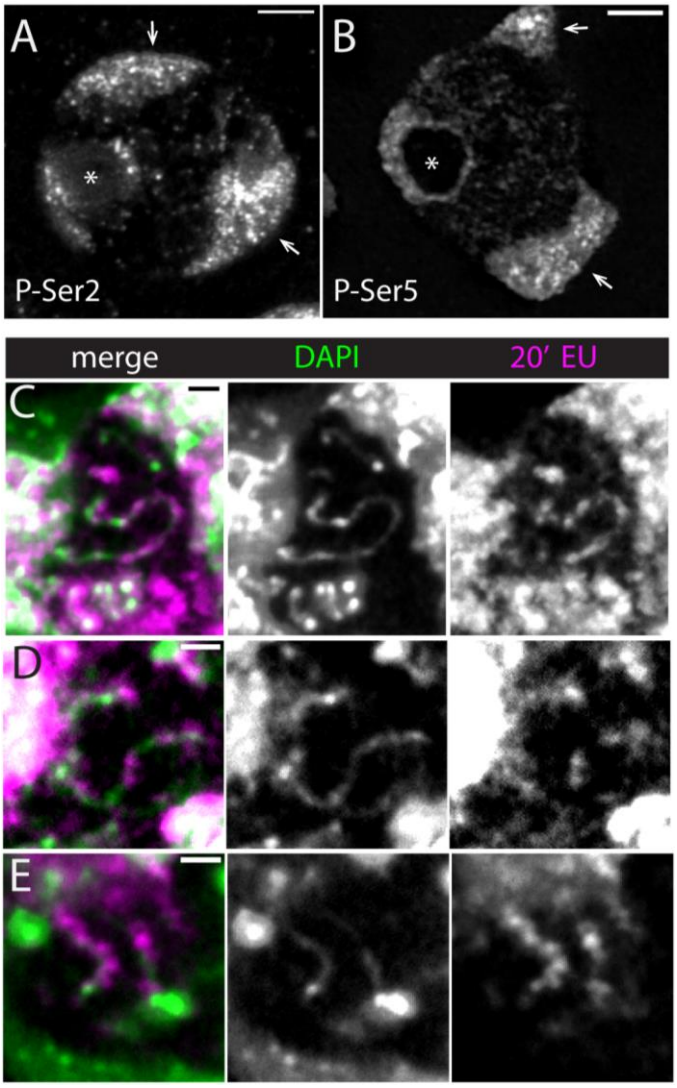

Figure 9. Polymerase and nascent transcription: confocal overview.
(A and B) Immunofluorescence images of RPol-PSer2 and RPol-PSer5 respectively in primary spermatocytes of larval testis whole-mounts. Single central confocal slices are shown. Arrows indicate autosome masses, asterisk indicates nucleolus, scale bars are 3 µm **(C-E)** show nascent RNA along DNA fibres. Nascent RNA labelled by 20 min incubation with EU (magenta) gives a blobby appearance along DAPI stained Y loops (green). **(C)** Maximum intensity projection of five confocal slices with a 150 nm step size captures a long Y loop section through the nucleoplasm. (D) and (E) are single slices. Scale bars are 1 µm.

bioRxiv preprint doi: https://doi.org/10.1101/2022.07.27.500934; this version posted October 19, 2022. The copyright holder for this preprint (which was not certified by peer review) is the author/funder, who has granted bioRxiv a license to display the preprint in perpetuity. It is made available under aCC-BY 4.0 International license.

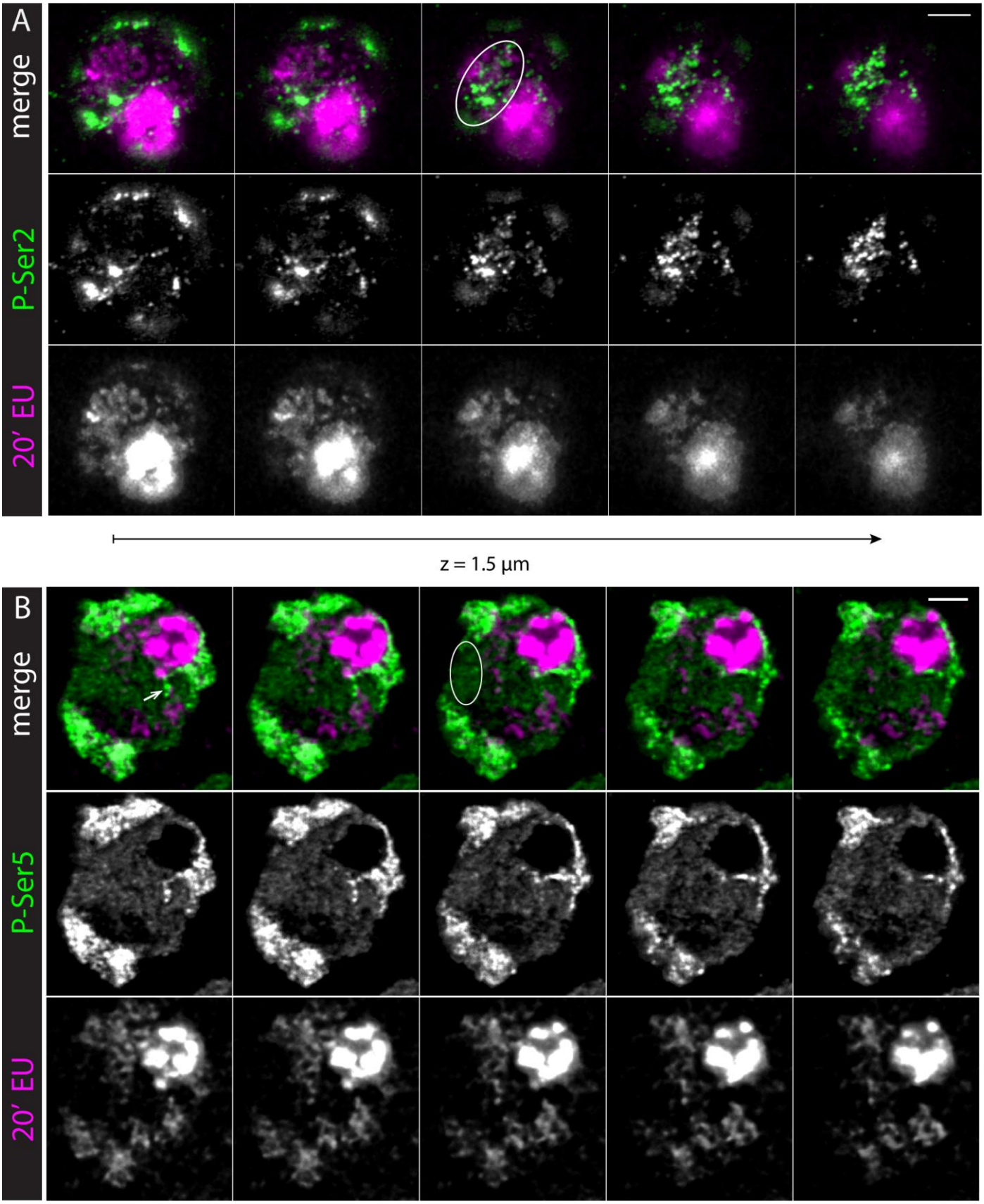

Figure 10. Differential association of nascent RNA with RPol-PSer2 and RPol-PSer5.
Primary spermatocytes in larval testes stained for EU to label nascent RNA (bottom rows, magenta in merge) after a 20 min incubation period and by immunolabelling for RPol-PSer2 **(A)** or RPol-PSer5 **(B)** (middle rows, green in merge). Consecutive confocal sections are shown from left to right covering approx. 1.5 µm along the z-axis. Scale bars, 3 µm. Nascent RNA accumulates around RPol-PSer2 along Y loops (ellipse in A), while RPol-PSer5 is frequently found without associated nascent RNA in the nucleoplasm (ellipse in B). Arrowhead in B points to prominent Y loop structure at the nucleolus, which is enriched with RPol-PSer5. Additionally, nascent RNA is enriched in chromosome masses in the nuclear periphery, which contain RPol with both CTD modifications, and in the nucleolus, where transcription is mostly performed by RPol1 (saturated round structure). Due to the high range of intensities some structures are saturated to visualize signals along the less dense Y loops.

bioRxiv preprint doi: https://doi.org/10.1101/2022.07.27.500934; this version posted October 19, 2022. The copyright holder for this preprint (which was not certified by peer review) is the author/funder, who has granted bioRxiv a license to display the preprint in perpetuity. It is made available under aCC-BY 4.0 International license.

Materials and Methods

Antibodies

Primary antibodies were: mouse anti-histone (core histones + H1, MabE71, Millipore), 1:1000; rabbit anti-RPol-PSer2 (ab238146, Abcam), 1:500; rabbit anti-RPol-PSer5 (ab76292, Abcam), 1:500 and rabbit anti-RPol-PSer2/5 (47355, Cell Signaling); 1:500. Secondary antibodies were from Invitrogen and used at 1:1000; goat anti-mouse Ig-Alexa Fluor 647 (A-21235), goat anti-rabbit Ig Alexa Fluor 488 (A-11008) and goat anti-rabbit Ig Alexa Fluor 568 (A-11011).

Spermatocyte Immunolabelling for STORM imaging

Testes of 0-5 day old male w^{1118} *Drosophila melanogaster* were dissected in PBS. The primary spermatocytes were isolated via gentle pipetting following collagenase digestion (Sigma-Aldrich C8051, 5 mg/ml in PBS for 5 min at room temperature) of the testes sheath, and fixed in 4% formaldehyde/PBS for 20 minutes at 37°C. The primary spermatocytes were filtered (Partec 04-004-2327) and seeded onto 35 mm high µ-dishes (Ibidi) for 30 minutes at room temperature. The cells were blocked overnight (1% Roche Western Blotting Reagent (WBR), Merck; 0.5% Triton X-100 in PBS). Following immunolabelling, the cells were fixed (2% formaldehyde) for 20 minutes at room temperature and stored in PBS at 4°C. To control for under-labelling of structures, we tested a range of antibody concentrations and found no significant difference in the observed nucleosome or RPol distribution.

STORM Imaging

Cells were imaged using a Zeiss Elyra 7, at 30°C using a BP490-560/LP640 filter. The STORM imaging buffer was as described in Peters et al., 2018 (43), adapted from (44,45). For dual-labelled samples with both Alexa Fluor 647 and 568, the cameras were aligned before each session using beads, or co-labelled structures on the cell dish (Suppl Fig 1). Varying numbers of frames (between 20,000 and 50,000 frames) were taken to optimally capture the signal for the biological structure imaged. There was no observed difference between quantification of the Y loops across different frame numbers above 20,000 frames therefore we concluded that the chromatin structure was saturated beyond this point. The exposure time used was 30 ms, using both the 561, and 640 laser at ~ 10 kW/cm^2 laser power throughout. The 488 laser was used at increasing power throughout image acquisition to recover fluorophores from the triple dark state, using ~ 70 - 100 W/cm^2 power. We found the 488 nm laser performed better on our microscope system as it gave a higher signal to noise than the commonly used 405 nm activatory laser.

STORM Buffers

Pyranose Oxidase Enzyme Storage buffer: PIPES (Sigma P-6757) 24 mM, $MgCl_2$ (Sigma M8266) 4 mM, EGTA (Bioserv BS-7249E) 2 mM, Glycerol (Sigma G5516) 30% v/v in dH_2O (pH 8.4). 250U Pyranose Oxidase enzyme (Sigma P4234) was added to 1.25 ml of enzyme storage buffer, mixed well then aliquoted into 75 µl tubes for storage at -20°C.

Pyranose Oxidase Imaging Base buffer: Tris buffer pH 8.5 (Jena Bioscience BU-124L-84) 50 mM, NaCl (Fisher Scientific 7647) 10 mM, Glucose (Sigma G8270) 0.56 M in dH_2O.

Pyranose Oxidase Final Imaging buffer: to 2784 µl Imaging Base Buffer was added 75 µl Pyranose Oxidase in Enzyme Storage Buffer (5 U/ml), 150 µl MEA (Sigma 30070) 1M (50 mM), 6 µl Catalase (Sigma C30)(40 µg/ml) and 30 µl COT (Sigma 138924) 200 mM in DMSO (2 mM).

Image analysis

Resulting .czi files were processed into localisation files using Zeiss ZEN Black software. The reconstructions were filtered based on precision (>5, <40 nm), photon number (>150, <8000), and point spread function (PSF) width (80 – 220nm) to improve the accuracy of the images and filter out noise. Drift correction was completed using the model-based drift correction, allowing an automatic selection of references points, a maximum of 21. The images were visualised using the "molecule density" option, which displays the localisations according to the density of neighbouring points, as well as precision value. The final images were then converted into .tif files and imported into ImageJ for the addition of scale bars.

Cluster analysis

The STORM-ready fluorophores Alexa Fluor 568 and Alexa fluor 647, conjugated to the secondary antibodies used in this study blink throughout time when exposed to STORM buffer. The centres of these blinks were statistically recognised using Zen Black software SMLM processing. These central points, hereafter referred to as 'localisations' were then reconstructed into a final image. Localisations from multiple antibodies on labelled structures form clusters. To model the spatial aggregation of antibody labelled molecules, a protocol based on spatial statistics and clustering approaches was designed and implemented. First, a description of the average cluster was established using spatial statistics, then a clustering algorithm using the average cluster parameters provided by the initial spatial statistics further refined the description; finding the cluster centres and the deviation of clusters from the average model.

We hypothesized that single molecule localisations form clusters that can be described as a modified Thomas process (46). This model is similar to a Bayesian approach (27), where the origins ("parent points") of the clusters were assumed to be completely randomly distributed, and the localisations can be seen as samples from identical isotropic 2D normal distributions $N(o_i,\sigma)$ around the origins o_i. The modified Thomas process has a closed form pair correlation function (PCF):

$$g(r) = 1 + \frac{1}{K}\frac{1}{(4\pi\sigma_1^2)} exp\left(-\frac{r^2}{4\sigma_1^2}\right) \quad (1)$$

where σ characterises the size of the cluster and κ is the intensity of the parent process. The parameters σ,κ can be estimated from fitting eq. 1 to the empirical PCF obtained from the data. This approach resulted in a description of the average cluster.

To mitigate the particular issue of cluster clumping caused by histones following along a Y loop fibre (violating the assumption of complete spatial randomness for the parent cluster location), a double cluster model was considered: the origin points are not randomly distributed but form a modified Thomas process as well. The PCF in this case became:

$$g2(r) = 1 + \frac{1}{K\mu}\frac{1}{(4\pi\sigma_1^2)} exp\left(-\frac{r^2}{4\sigma_1^2}\right) + \frac{1}{K}\frac{1}{\left(4\pi\left(\sigma_2^2+\sigma_1^2\right)\right)} exp\left(\frac{-r^2}{4\left(\sigma_2^2+\sigma_1^2\right)}\right) \quad (2)$$

with σ_1 describing the parent cluster radius, σ_2 the scale of localisation clusters and μ the number of fluorophores per cluster. Goodness of fit was evaluated for each data selection, and the σ resulting from the best fitting cluster model (single-cluster, or double-cluster) was recorded for downstream cluster analysis. In order to identify and describe individual clusters, a mode-finding clustering algorithm, MeanShift was applied (28,29) using a MATLAB script based on (30).

The crucial parameter of MeanShift is the search radius, which was set to 2σ, as suggested in (47) and calculated for each individual dataset from the spatial statistics process. The other parameters used for MeanShift were as follows; weight 0.2, maximum iteration 50, minimum cluster size 15. The number of localisations and mean full width half maximum (FWHM) per identified clusters were recorded (the mean FWHM was considered in order to account for potential anisotropy of the clusters) and visualised using histogram and box and whisker plots (48). The quantification workflow can be summarised as follows: 1) A section of confident non-overlapping Y loop clusters was cropped into regions of interest (ROIs), as shown in Figure 3 B; 2) The 2σ of the average cluster model for each individual cropped dataset was quantified using spatial statistics to best set up MeanShift for robust clustering; 3) MeanShift was run on each dataset with the matching 2σ search radius parameter, and each cluster within each dataset was assigned a mean FWHM value; 4) all of the results were pooled and displayed as histograms and box and whisker plots (Total experiments = 7, total cells = 12, total Y loop clusters quantified = 2473).

Nucleosome per cluster calculation

The volume of a single nucleosome was calculated as a disc of radius 5.5 nm, and height 5 nm., giving a nucleosome volume of 475.2 nm^3. The maximum number of nucleosomes within a given sphere volume for each cluster was then calculated by dividing the cluster volume by the nucleosome volume.

EU labelling and immunofluorescence of larval *Drosophila* testes

Drosophila melanogaster (w^{1118}) larval testes were dissected into ice-cold Schneider's medium (Gibco) supplemented with 10 % FBS (Biosera) and 1x Penicillin/Streptomycin (Sigma). For EU labelling and click chemistry the Click-iT RNA Imaging Kit (Molecular Probes, Inc., C10330) was used according to the manufacturer's protocol with minor modifications. Briefly, testes were incubated in medium containing 1 mM 5-ethynyl uridine (EU) for 20 min at 25°C and fixed with 3.7% Formaldehyde (Sigma), 1 % Triton X-100 (Sigma) in PBS (Oxoid). For detection, the incorporated EU was ligated to Alexa Fluor 647 azide via the click reaction. For immunofluorescence testes were blocked

bioRxiv preprint doi: https://doi.org/10.1101/2022.07.27.500934; this version posted October 19, 2022. The copyright holder for this preprint (which was not certified by peer review) is the author/funder, who has granted bioRxiv a license to display the preprint in perpetuity. It is made available under aCC-BY 4.0 International license.

and permeabilized with 1 % Western Blocking Reagent (WBR, Merck), 0.5 % Triton X-100 in PBS at 4-8°C over night, incubated with primary antibodies in PBS containing 1 % WBR, washed with 0.1 % Tween 20 (Sigma-Aldrich) in PBS, incubated with secondary antibodies, washed with 0.1 % Tween 20 in PBS, post-fixed for 20 min with 3.7 % Formaldehyde at room temperature and mounted on microscopy slides with AF1 (Citifluor).

Imaging was performed on a Leica TCS SP8 confocal microscope with an HC PL APO CS2 63x/1.40 OIL objective, 1 AU pinhole size, voxel size of 42x42x140 or 71x71x299 nm, 4x line averaging using 488 Argon and 633 nm HeNe lasers, and GaAsP Hybrid Detectors (HyD). The Alexa Fluor 488 channel was acquired sequentially with the 647 channel. Data were denoised with Noise2Void (3D) (49) using ZeroCostDL4Mic (50); a comparison with the raw data is shown in Suppl Fig 1. For N2V3D model training 5-slice stacks from the bottom, centre and top of the unprocessed stack were used and training quality was assessed by comparing training and validation loss, and by visual examination of raw and denoised images. Figures were arranged and contrast adjusted with Fiji (51), Adobe Illustrator and Photoshop.

Acknowledgements

We thank Sherif El Sharnouby and Levente Kovacs for help with spermatocyte labelling methods, Ruby Peters for help with dual label STORM and Martin Lenz for expert microscopy support. The BioRxiv MS Word template is from Christian L. Ebbesen.

Author Contributions

RW conceived the project; RW and KOH supervised the project; MLB, SAK and SAR carried out the experiments, MLB and LM carried out the analysis. MLB, RW, SAK and LM wrote the manuscript. All authors read and approved the final manuscript.

Funding

The work was supported by the Biotechnology and Biological Sciences Research Council Grant (BB/S00758X/1) to RW, by a Cambridge BBSRC-DTP studentship to MLB and an Engineering and Physical Sciences Research Council Grant (EP/R025398/1) to LM. The funders had no role in the study design, data collection and analysis, decision to publish, or preparation of the manuscript.

Competing interests

The authors have declared that no competing interests exist.

References

1. Shaban HA, Barth R, Bystricky K. Navigating the crowd: visualizing coordination between genome dynamics, structure, and transcription. Genome Biol. 2020 Dec;21(1):1–18.
2. Grubert F, Srivas R, Spacek DV, Kasowski M, Ruiz-Velasco M, Sinnott-Armstrong N, et al. Landscape of cohesin-mediated chromatin loops in the human genome. Nature. 2020 Jul;583(7818):737–43.
3. Rao SSP, Huntley MH, Durand NC, Stamenova EK, Bochkov ID, Robinson JT, et al. A 3D Map of the Human Genome at Kilobase Resolution Reveals Principles of Chromatin Looping. Cell. 2014 Dec 18;159(7):1665–80.
4. Dixon JR, Gorkin DU, Ren B. Chromatin Domains: The Unit of Chromosome Organization. Molecular Cell. 2016 Jun 2;62(5):668–80.
5. Sexton T, Yaffe E, Kenigsberg E, Bantignies F, Leblanc B, Hoichman M, et al. Three-dimensional folding and functional organization principles of the Drosophila genome. Cell. 2012 Feb 3;148(3):458–72.
6. Lieberman-Aiden E, van Berkum NL, Williams L, Imakaev M, Ragoczy T, Telling A, et al. Comprehensive mapping of long range interactions reveals folding principles of the human genome. Science. 2009 Oct 9;326(5950):289–93.
7. Cremer T, Cremer C. Chromosome territories, nuclear architecture and gene regulation in mammalian cells. Nat Rev Genet. 2001 Apr;2(4):292–301.
8. Boettiger A, Murphy S. Advances in chromatin imaging at kilobase-scale resolution. Trends Genet. 2020 Apr;36(4):273–87.
9. Xie, L., Liu, Z. Single-cell imaging of genome organization and dynamics. Molecular Systems Biology. 2021 Jul;17(7):e9653.
10. Ou HD, Phan S, Deerinck TJ, Thor A, Ellisman MH, O'Shea CC. ChromEMT: Visualizing 3D chromatin structure and compaction in interphase and mitotic cells. Science. 2017 Jul 28;357(6349).
11. Nozaki T, Imai R, Tanbo M, Nagashima R, Tamura S, Tani T, et al. Dynamic Organization of Chromatin Domains Revealed by Super-Resolution Live-Cell Imaging. Mol Cell. 2017 Jul 20;67(2):282-293.e7.
12. Ricci MA, Manzo C, García-Parajo MF, Lakadamyali M, Cosma MP. Chromatin Fibers Are Formed by Heterogeneous Groups of Nucleosomes In Vivo. Cell. 2015 Mar 12;160(6):1145–58.
13. Boettiger AN, Bintu B, Moffitt JR, Wang S, Beliveau BJ, Fudenberg G, et al. Super-resolution imaging reveals distinct chromatin folding for different epigenetic states. Nature. 2016 Jan;529(7586):418–22.
14. Xu J, Ma H, Jin J, Uttam S, Fu R, Huang Y, et al. Super-Resolution Imaging of Higher-Order Chromatin Structures at Different Epigenomic States in Single Mammalian Cells. Cell Reports. 2018 Jul 24;24(4):873–82.
15. Callan, H.G. Lampbrush Chromosomes. Springer Berlin, Heidelberg; 1986. (Mol Biol Biochem Biophys; vol. 36).
16. Chambeyron S, Bickmore WA. Chromatin decondensation and nuclear reorganization of the HoxB locus upon induction of transcription. Genes Dev. 2004 May 15;18(10):1119–30.
17. Daneholt B. Transcription in polytene chromosomes. Cell. 1975 Jan 1;4(1):1–9.
18. Müller WG, Walker D, Hager GL, McNally JG. Large-scale chromatin decondensation and recondensation regulated by transcription from a natural promoter. J Cell Biol. 2001 Jul 9;154(1):33–48.
19. Winick-Ng W, Kukalev A, Harabula I, Zea-Redondo L, Szabó D, Meijer M, et al. Cell-type specialization is encoded by specific chromatin topologies. Nature. 2021 Nov;599(7886):684–91.
20. Bonaccorsi S, Pisano C, Puoti F, Gatti M. Y Chromosome Loops in Drosophila Melanogaster. Genetics. 1988 Dec;120(4):1015–34.
21. Cenci, G., Bonaccorsi, S., Pisano, C., Verni, F. G M. Chromatin and microtubule organization during premeiotic, meiotic and early postmeiotic stages of Drosophila melanogaster spermatogenesis. J Cell Sci. 1994;107:3521–34.
22. Carvalho AB, Dobo BA, Vibranovski MD, Clark AG. Identification of five new genes on the Y chromosome of Drosophila melanogaster. Proceedings of the National Academy of Sciences. 2001 Nov 6;98(23):13225–30.
23. Goldstein LS, Hardy RW, Lindsley DL. Structural genes on the Y chromosome of Drosophila melanogaster. Proceedings of the National Academy of Sciences. 1982 Dec;79(23):7405–9.
24. Hardy RW, Tokuyasu KT, Lindsley DL. Analysis of spermatogenesis in Drosophila melanogaster bearing deletions for Y-chromosome fertility genes. Chromosoma. 1981 Aug 1;83(5):593–617.
25. Rust MJ, Bates M, Zhuang X. Stochastic optical reconstruction microscopy (STORM) provides sub-diffraction-limit image resolution. Nat Methods. 2006 Oct;3(10):793–5.
26. Ester M, Kriegel HP, Sander J, Xu X. A density-based algorithm for discovering clusters in large spatial databases with noise. In: Proceedings of the Second International Conference on Knowledge Discovery and Data Mining. Portland, Oregon: AAAI Press; 1996. p. 226–31. (KDD'96).
27. Griffié J, Shannon M, Bromley CL, Boelen L, Burn GL, Williamson DJ, et al. A Bayesian cluster analysis method for single-molecule localization microscopy data. Nat Protoc. 2016 Dec;11(12):2499–514.
28. Comaniciu D, Meer P. Mean shift: a robust approach toward feature space analysis. IEEE Transactions on Pattern Analysis and Machine Intelligence. 2002 May;24(5):603–19.
29. Fukunaga K, Hostetler L. The estimation of the gradient of a density function, with applications in pattern recognition. IEEE Transactions on Information Theory. 1975 Jan;21(1):32–40.
30. Piotr Dollar. Piotr's Computer Vision Matlab Toolbox (PMT) [Internet]. Available from: https://github.com/pdollar/toolbox
31. Sengupta P, Jovanovic-Talisman T, Skoko D, Renz M, Veatch SL, Lippincott-Schwartz J. Probing protein heterogeneity in the plasma membrane using PALM and pair correlation analysis. Nat Methods. 2011 Sep 18;8(11):969–75.
32. Veatch SL, Machta BB, Shelby SA, Chiang EN, Holowka DA, Baird BA. Correlation Functions Quantify Super-Resolution Images and Estimate Apparent Clustering Due to Over-Counting. PLOS ONE. 2012 Feb 27;7(2):e31457.
33. Cisse II, Izeddin I, Causse SZ, Boudarene L, Senecal A, Muresan L, et al. Real-Time Dynamics of RNA Polymerase II Clustering in Live Human Cells. Science. 2013 Aug 9;341(6146):664–7.
34. Nojima T, Rebelo K, Gomes T, Grosso AR, Proudfoot NJ, Carmo-Fonseca M. RNA Polymerase II Phosphorylated on CTD Serine 5 Interacts with the Spliceosome during Co-transcriptional Splicing. Molecular Cell. 2018 Oct 18;72(2):369-379.e4.
35. Venkat Ramani MK, Yang W, Irani S, Zhang Y. Simplicity is the Ultimate Sophistication—Crosstalk of Post-translational Modifications on the RNA Polymerase II. Journal of Molecular Biology. 2021 Jul;433(14):166912.
36. Castells-Garcia A, Ed-daoui I, González-Almela E, Vicario C, Ottestrom J, Lakadamyali M, et al. Super resolution microscopy reveals how elongating RNA polymerase II and nascent RNA interact with nucleosome clutches. Nucleic Acids Research. 2022 Jan 11;50(1):175–90.
37. Maeshima K, Rogge R, Tamura S, Joti Y, Hikima T, Szerlong H, et al. Nucleosomal arrays self-assemble into supramolecular globular structures lacking 30-nm fibers. EMBO J. 2016 May 17;35(10):1115–32.

bioRxiv preprint doi: https://doi.org/10.1101/2022.07.27.500934; this version posted October 19, 2022. The copyright holder for this preprint (which was not certified by peer review) is the author/funder, who has granted bioRxiv a license to display the preprint in perpetuity. It is made available under aCC-BY 4.0 International license.

38. Cook PR. The organization of replication and transcription. Science. 1999 Jun 11;284(5421):1790–5.
39. Liu LF, Wang JC. Supercoiling of the DNA template during transcription. Proc Natl Acad Sci U S A. 1987 Oct;84(20):7024–7.
40. Hari-Gupta Y, Fili N, dos Santos Á, Cook AW, Gough RE, Reed HCW, et al. Myosin VI regulates the spatial organisation of mammalian transcription initiation. Nat Commun. 2022 Mar 15;13(1):1346.
41. Leidescher S, Ribisel J, Ullrich S, Feodorova Y, Hildebrand E, Galitsyna A, et al. Spatial organization of transcribed eukaryotic genes. Nat Cell Biol. 2022 Mar;24(3):327–39.
42. Redhouse JL, Mozziconacci J, White RAH. Co-transcriptional architecture in a Y loop in Drosophila melanogaster. Chromosoma. 2011 Aug;120(4):399–407.
43. Peters R, Griffié J, Burn GL, Williamson DJ, Owen DM. Quantitative fibre analysis of single-molecule localization microscopy data. Sci Rep. 2018 Jul 10;8(1):10418.
44. Olivier N, Keller D, Gönczy P, Manley S. Resolution doubling in 3D-STORM imaging through improved buffers. PLoS One. 2013;8(7):e69004.
45. Swoboda M, Henig J, Cheng HM, Brugger D, Haltrich D, Plumeré N, et al. Enzymatic Oxygen Scavenging for Photostability without pH Drop in Single-Molecule Experiments. ACS Nano. 2012 Jul 24;6(7):6364–9.
46. Ilian J, Penttinen A, Stoyan H, Stoyan D. Statistical Analysis and Modelling of Spatial Point Patterns [Internet]. Wiley; 2008. Available from: http://www.wiley.com/en-gb/Statistical+Analysis+and+Modelling+of+Spatial+Point+Patterns-p-9780470014912
47. Huang K, Fu X, Sidiropoulos ND. On Convergence of Epanechnikov Mean Shift [Internet]. arXiv; 2017. Available from: http://arxiv.org/abs/1711.07441
48. Lansey, J.C. Plot and compare histograms; pretty by default [Internet]. Available from: https://uk.mathworks.com/matlabcentral/fileexchange/27388-plot-and-compare-histograms-pretty-by-default
49. Krull A, Buchholz TO, Jug F. Noise2Void - Learning Denoising from Single Noisy Images. arXiv:181110980 [cs]. 2019 Apr 5;
50. von Chamier L, Laine RF, Jukkala J, Spahn C, Krentzel D, Nehme E, et al. Democratising deep learning for microscopy with ZeroCostDL4Mic. Nat Commun. 2021 Apr 15;12(1):2276.
51. Schindelin J, Arganda-Carreras I, Frise E, Kaynig V, Longair M, Pietzsch T, et al. Fiji: an open-source platform for biological-image analysis. Nat Methods. 2012 Jul;9(7):676–82.

bioRxiv preprint doi: https://doi.org/10.1101/2022.07.27.500934; this version posted October 19, 2022. The copyright holder for this preprint (which was not certified by peer review) is the author/funder, who has granted bioRxiv a license to display the preprint in perpetuity. It is made available under aCC-BY 4.0 International license.

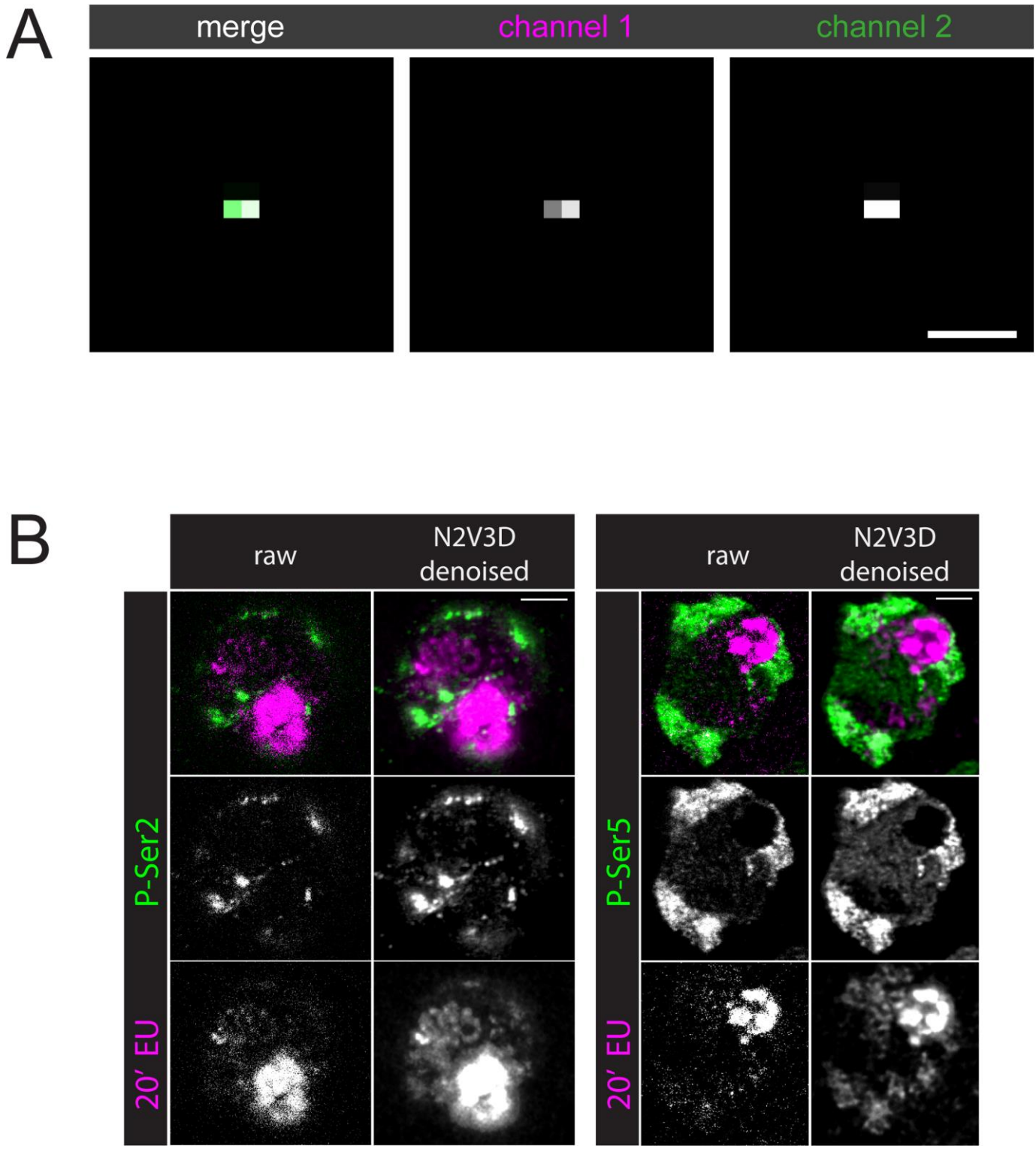

Suppl. Figure 1
(A) Demonstration of the outcome of manual alignments of the camera using a 100 nm bead. The super-resolution SMLM analysis process is run on the bead, producing a few localisations at the central position of the bead. Then, the misalignment between the camera is corrected, and the analysis re-tried. This process is repeated until the two resulting localisations in both cameras are directly on top of each other, showing that the cameras are aligned. Scale bar = 100 nm. **(B)** Comparison of raw and N2V3D denoised images. Scale bars, 3 µm. Corresponds to Fig 10.